

Enhanced Photocatalytic Water Splitting of Hydrous $LiCa_2Ta_3O_{10}$ Prepared by Hydrothermal Treatment

Tomohiro Mitsuyama, Akiko Tsutsumi, Takakazu Hata, Keita Ikeue, and Masato Machida*

Department of Nano Science and Technology, Graduate School of Science and Technology, Kumamoto University, 2-39-1 Kurokami, Kumamoto 860-8555

Received November 15, 2007; E-mail: machida@chem.kumamoto-u.ac.jp

Hydration behavior of $A'Ca_2Ta_3O_{10}$ ($A' =$ Cs, Rb, K, Na, and Li) was studied focusing on the photocatalytic activity for overall water splitting under UV-irradiation. Interlayer hydration was only observed for $A' =$ Na and Li, which possess a large enthalpy of hydration (ΔH_h°). A Na phase readily yielded a stable hydrous phase even at ambient temperature, whereas a Li phase required hydrothermal treatment at $\geq$160 °C. This is consistent with the fact that the Na phase kept its space group (*I*4/*mmm*) unchanged during hydration, whereas the Li phase changed from *I*4/*mmm* to *P*4/*mmm*. Hydration of the Li phase doubled the rate of photocatalytic gas evolution ($\geq$700 μmol-H_2 h^{-1}) in the presence of 0.5 wt % Ni load, which was the highest in the series of $A'Ca_2Ta_3O_{10}$. It was demonstrated that the hydrated interlayer is an efficient structural modification to enhance the photocatalytic activity of the ion-exchangeable layered perovskite-type oxides.

Ion-exchangeable layered perovskite-type titanates, niobates, and tantalates with d^0 electronic configuration are well-known as active photocatalysts for overall water splitting under UV-irradiation.[1–17] For understanding the structure–activity relationship of these compounds, the role of interlayer space is of general interest because its hydration is found to significantly affect photocatalytic activity. It has been reported that several layered perovskites, such as $K_4Nb_6O_{17}$[4,8] and $K_2La_2Ti_3O_{10}$,[7] are highly active, because their interlayer space is easily hydrated to produce active sites responsible for photocatalytic reactions. We have studied the electronic structure as well as crystal structure of Dion–Jacobson (D–J) type triple layered tantalate, $A'Ca_2Ta_3O_{10}$.[17] The tantalates exhibit different photocatalytic activity for overall water splitting depending on the interlayer monovalent cations (A'). The Na phase ($A' =$ Na) exhibited a high rate of gas evolution (H_2: ≈300 μmol h^{-1}, 0.5 wt % Ni load), compared to the Cs phase (H_2: <100 μmol h^{-1}, 0.5 wt % Ni load). These two compounds showed contrasting behavior in hydration; the Na phase is easily hydrated in contrast to a totally anhydrous Cs phase. The rapid and reversible hydration/dehydration of the Na phase caused by the high mobility of water molecules in the interlayer space may affect the photocatalytic activity, but further discussion requires the structure–activity relationship for a series of compounds, $A'Ca_2Ta_3O_{10}$ ($A' =$ Cs, Rb, K, Na, and Li).

In the present work, we thus studied the hydration behavior of $A'Ca_2Ta_3O_{10}$ in relation to their photocatalytic activity for water splitting. We have especially noted the hydration of $LiCa_2Ta_3O_{10}$ as an efficient structural modification to enhance photocatalytic activity. To intercalate water molecules between the triple tantalate layers of the present phase, hydrothermal treatment was applied under different conditions. As treated compounds were characterized by means of XRD, TG, SEM, UV–vis, and FT-IR and applied to photocatalytic water splitting. Enhanced photocatalytic activity after hydrothermal treatment is discussed with a focus on the role of interlayer water and the chemical state of Ni to elucidate the structure–activity relationship of the present system.

Experimental

Powder samples of $A'Ca_2Ta_3O_{10}$ ($A' =$ Cs and Rb) were prepared by a conventional solid-state reaction using mixtures of A'_2CO_3, $CaCO_3$, and Ta_2O_5 at 1000 °C. An excess of 50 mol % of A'_2CO_3 was used to compensate the loss due to vaporization during heating. The calcined $CsCa_2Ta_3O_{10}$ was heated in molten nitrate ($A'NO_3$) at different temperatures, 430, 400, and 280 °C for $A' =$ K, Na, and Li, respectively, to convert to each alkali metal-exchanged forms. The exchanged samples were washed with distilled deionized water and dried in vacuo at room temperature.

0.5 wt % Ni was loaded onto $A'Ca_2Ta_3O_{10}$ using aqueous $Ni(NO_3)_2$ solution by impregnation. Ni-loaded samples were heated at 500 °C for 2 h in a stream of O_2 and subsequently at 500 °C for 2 h in H_2. As reduced 0.5 wt % Ni-loaded samples were partially reoxidized in O_2 at 200 °C prior to the photocatalytic reactions. Also, 0.5 wt % Ni-loaded samples were hydrothermally treated as follows. Reduced 0.5 wt % Ni/$LiCa_2Ta_3O_{10}$ powders (0.30 g) and distilled deionized water (40 mL) were placed in an inner-lined stainless-steel autoclave having a 50-mL Teflon inner vessel. The mixture was heated at 160–180 °C for 2–18 h without stirring and then cooled to room temperature. The treated samples were collected by centrifuge, dried in vacuo at room temperature, and applied to the photocatalytic reaction without reoxidation in O_2 at 200 °C.

Crystal structure and chemical composition of as prepared samples were determined by powder X-ray diffraction (XRD, Rigaku Multiflex) and X-ray fluorescence (XRF, Horiba MESA-500W). Thermogravimetric analysis (TG, Rigaku 8120) was performed to determine the amount of interlayer water in a flow of N_2 at a heating rate of 10 °C min^{-1}. Microstructure was observed by SEM (JEOL, JSM-6060LV). Diffuse reflectance spectra were recorded

Published on the web March 13, 2008; doi:10.1246/bcsj.81.401

Table 1. Properties of Alkali Cations and Photocatalytic Activity of 0.5 wt % Ni-Loaded $A'Ca_2Ta_3O_{10}\cdot nH_2O$ (A′ = Cs, Rb, K, Na, and Li)

A′	r[a)]/nm	ΔH_h°[b)]/kJ mol^{-1}	n[c)]/mol mol^{-1}	H_2[d)]/μmol h^{-1}	O_2[d)]/μmol h^{-1}
Li	0.068	−536.3	0	356	194
Na	0.098	−420.8	1.92	293	162
K	0.133	−337.1	0	177	81
Rb	0.148	−312.5	0	180	91
Cs	0.167	−287.3	0	89	53

a) Ionic radius. b) Enthalpy of hydration for A′. c) Hydration number. d) Rates of photocatalytic gas evolution, photocatalyst 0.20 g, pure water 200 mL, inner-irradiation quartz vessel, 400-W high pressure Hg lamp. The Ni-loaded photocatalysts were reoxidized in O_2 at 200 °C after H_2 reduction.

with a UV–vis spectrometer (Jasco, V-550) to determine optical band gap energy.

Photocatalytic water splitting reactions were carried out in an inner-irradiation type quartz vessel connected to a closed gas-circulating system. Photocatalyst powder (0.20 g) in 200 mL of pure water dispersed by magnetic stirrer was photo-irradiated with a 400-W high-pressure mercury lamp. The rates of H_2 and O_2 evolution were determined using a gas chromatograph (Shimadzu GC-8A, TCD, Ar carrier, MS-5A).

Results and Discussion

Effect of Interlayer Cations on Hydration Behavior. A series of $A'Ca_2Ta_3O_{10}$ (A′ = Cs, Rb, K, Na, and Li) were obtained as single phases by solid-state reactions (A′ = Cs and Rb) or ion-exchange of $CsCa_2Ta_3O_{10}$ in corresponding molten nitrates (A′ = K, Na, and Li). X-ray fluorescence analysis showed that more than 99% of Cs could be replaced by K, Na, or Li. As was revealed by Toda et al.,[18,19] these compounds exhibited a similar layered structure, which is constructed by alternative stacking of a triple perovskite slab, $[Ca_2Ta_3O_{10}]^-$, and A'^+ ions. However, their space groups are classified into three groups, A′ = Cs and Rb ($P4/mmm$), K ($C222$), and Na and Li ($I4/mmm$), depending on the relative arrangement of adjacent triple perovskite layers.

Table 1 shows the hydration number (n in $A'Ca_2Ta_3O_{10}\cdot nH_2O$) of the prepared phases. It should be noted that the Na phase was only in the form of a hydrate ($n \approx 2$), whereas the other phases were stable in anhydrous states ($n = 0$). As was reported in our previous paper,[17] the hydration of the Na phase takes place readily even by absorbing atmospheric moisture at room temperature, whereas the parent Cs phase was highly resistant to hydration both in vapor and liquid phases. Water molecules are accommodated into the interlayer of the Na phase, occupying the sites surrounding Na ions. The difference of such hydration behavior should therefore be associated with the enthalpy of hydration (ΔH_h°)[20] of A′; hydration is expected to be thermodynamically favorable for A′ ions having large ΔH_h° (Table 1). This is reasonable considering the anhydrous property of the tantalates containing A′ = K, Rb, and Cs. Nevertheless, this is not consistent with the fact that the Li phase forms a stable anhydrous phase in spite of the largest ΔH_h° of Li^+. One plausible reason for the anhydrous behavior is that the intercalation of water would kinetically be prohibited by the small interlayer distance because of the minimal ionic radius of Li^+ (0.068 nm).

The optical band gap energy of $A'Ca_2Ta_3O_{10}$ was almost the same, in the range of 4.2–4.3 eV, because the valence band and the conduction band consist commonly of O2p and Ta5d, respectively, and A′ ions do not contribute to both bands responsible for photocatalytic processes.[17] The BET surface area ($\leq 5\ m^2\ g^{-1}$) and particle size (0.5–1 μm) are indicative of negligible differences in their microstructure. Photocatalytic activity for water splitting was measured for 0.5 wt % Ni-loaded $A'Ca_2Ta_3O_{10}$ under UV irradiation (Table 1). Here, the Ni-loaded photocatalysts were reduced in H_2 at 500 °C and subsequently reoxidized in O_2 at 200 °C. As is evident from Table 1, the activity was strongly dependent on A′, in the order of Cs < Rb ≈ K < Na < Li. The reason for the A′ dependence of photocatalytic activity is not clear at this stage, but it should be pointed out that the high photocatalytic activity for A′ = Na is susceptible to its hydrated interlayer.[17] The hydration of the Li phase appears therefore of great interest as a useful structural modification to enhance further the photocatalytic activity for water splitting.

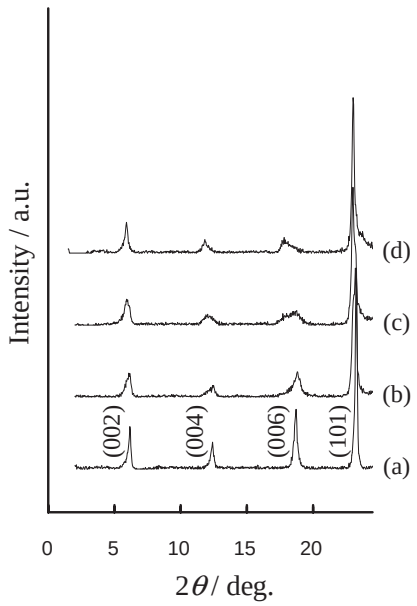

Fig. 1. XRD patterns of $LiCa_2Ta_3O_{10}$ (a) before and after hydrothermal treatment at 180 °C for (b) 2, (c) 6, and (d) 12 h.

Hydrothermal Treatment of Li Phase. Because hydration of the Li phase appears to be kinetically prohibited as above mentioned, hydrothermal treatment was applied. Figure 1 shows the XRD patterns of $LiCa_2Ta_3O_{10}$ before

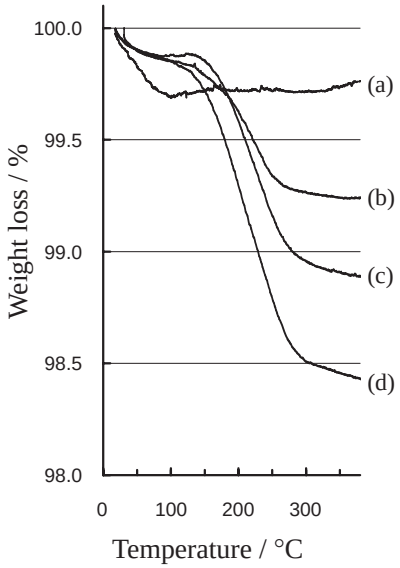

Fig. 2. TG curves of $LiCa_2Ta_3O_{10}$ in an N_2 flow (a) before and after hydrothermal treatment at 180 °C for (b) 2, (c) 6, and (d) 12 h. Heating rate: 10 °C min^{-1}.

and after hydrothermal treatment at 180 °C. Clearly, the (00*l*) reflections were shifted towards lower 2θ with an increase of time, leading to an increase of interlayer spacing ($d = d_{002}$) from 1.43 to 1.49 nm. In contrast to the expansion along the *c* axis, the lattice dimension along the *ab* direction remained unchanged, suggesting the occurrence of water intercalation. FT-IR measurement indicated the appearance of bands due to OH stretching (ν_{OH}) at 3450 cm^{-1} and HOH bending (δ_{HOH}) at 1640 cm^{-1} (Supporting Information). Figure 2 shows TG curves of $LiCa_2Ta_3O_{10}$ before and after hydrothermal treatment at 180 °C. Weight loss at the beginning (≤100 °C) was caused by desorption of physisorbed water. Untreated $LiCa_2Ta_3O_{10}$ showed no more weight loss, whereas the hydrothermally treated material gave rise to a second weight loss at 100–300 °C, which increased with elongation of time of the treatment. Parallel mass spectroscopy measurement of gas evolution from the sample suggested the occurrence of water desorption in that temperature range. We have also conducted in situ XRD measurements during heating at constant rate, which confirmed that the hydrothermally treated sample exhibited a shift of (00*l*) reflections to higher 2θ at 100–300 °C because of deintercalation of water molecules. These results clearly indicate that interlayer hydration of $LiCa_2Ta_3O_{10}$ can be achieved under hydrothermal conditions. The hydration number was in the range $0.09 \leq n \leq 0.7$, depending on the temperature and time for the hydrothermal treatment. These values are smaller than that for $NaCa_2Ta_3O_{10}$ ($n \approx 2$), probably because of the narrow interlayer space due to the small size of Li^+. Although hydrothermal treatment was applied to other anhydrous $A'Ca_2Ta_3O_{10}$ ($A' =$ Cs, Rb, and K), hydration of interlayers could not be observed probably because of the small ΔH_h° as above mentioned.

Figure 3 compares the assignment of XRD peaks of anhydrous $LiCa_2Ta_3O_{10}$ (a) and $LiCa_2Ta_3O_{10}\cdot 0.64H_2O$ (b), which was obtained by hydrothermal treatment at 180 °C for 12 h. The diffraction peaks observed for anhydrous $LiCa_2Ta_3O_{10}$

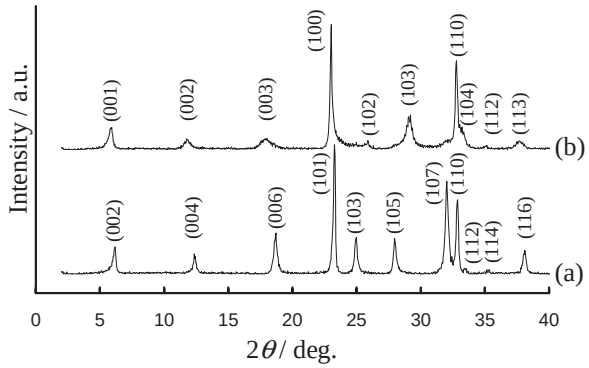

Fig. 3. Assignment of XRD peaks of (a) anhydrous and (b) hydrous $LiCa_2Ta_3O_{10}$. The hydrous phase was prepared by hydrothermal treatment at 180 °C for 12 h.

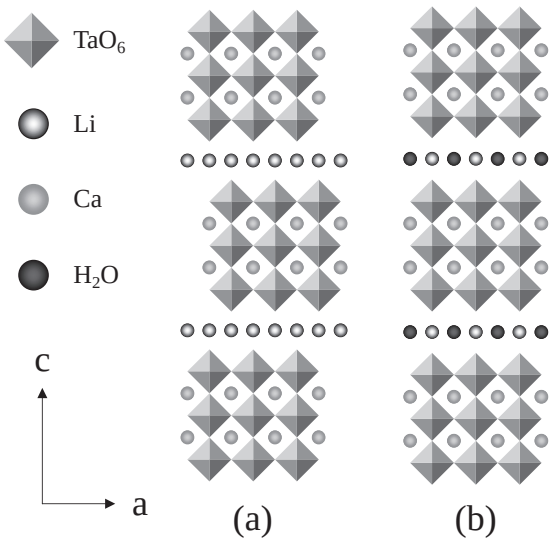

Fig. 4. Crystal structure models of (a) anhydrous and (b) hydrous $LiCa_2Ta_3O_{10}$.

were indexed with a body-centered tetragonal lattice ($I4/mmm$, $a_0 = 0.3850$ nm, $c_0 = 2.8362$ nm) as previously reported.[19] The hydration caused the appearance of a (100) peak with simultaneous disappearance of original peaks due to (101), (103), (105), and (107) consistent with the change of the space group from $I4/mmm$ to a $P4/mmm$. On the basis of a tetragonal unit cell with the $P4/mmm$ symmetry, all of the observed diffraction peaks in the 2θ range of 5–70° could be indexed by the least-squares fitting method with the lattice parameters, $a_0 = 0.3853$ nm, $c_0 = 1.5099$ nm. The structure models of anhydrous and hydrous $LiCa_2Ta_3O_{10}$ phases are shown schematically in Fig. 4. Each structure is constructed by alternative stacking of a triple-corner-shared TaO_6 octahedra and a Li layer along *c* axis. The transformation from $I4/mmm$ to $P4/mmm$ is explained by the displacement of adjacent perovskite slabs by $a/2$ along the [110] direction. Such structural change caused by hydration is in contrast to the Na phase, the original space group ($I4/mmm$) of which was retained upon hydration/dehydration.[21] The different structural change may be associated with the small hydration number of the Li phase, $n < 1$, compared to $n \approx 2$ achieved for the Na phase.

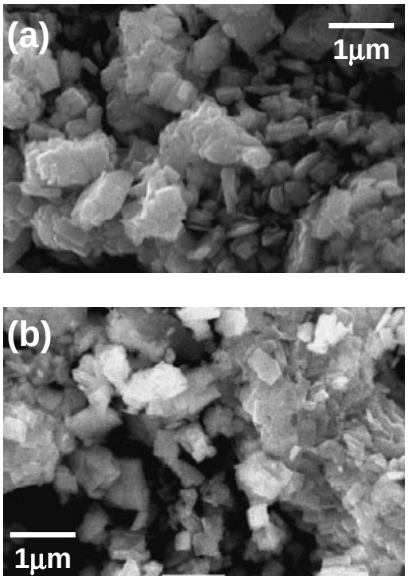

Fig. 5. SEM photographs of (a) anhydrous and (b) hydrous $LiCa_2Ta_3O_{10}$. The hydrous phase was prepared by hydrothermal treatment at 180 °C for 12 h.

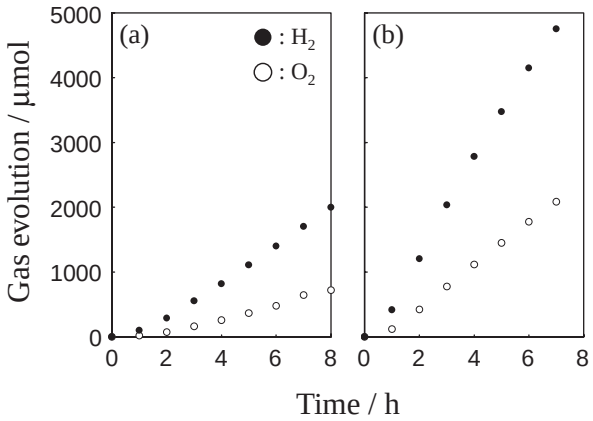

Fig. 6. Photocatalytic water splitting over 0.5 wt % Ni loaded (a) anhydrous and (b) hydrous $LiCa_2Ta_3O_{10}$. The hydrous phase was prepared by hydrothermal treatment at 160 °C for 12 h.

The reason for the displacement that occurred in hydration of the Li phase is not elucidated at this stage. However, a similar transformation accompanied by the displacement of adjacent perovskite slabs was reported by Hong et al.[22] for a hydrated D–J perovskite phase of $NaLa_2Ti_2TaO_{10}\cdot nH_2O$. A fully hydrated phase ($n = 2.0$, $I4/mmm$) is thermally dehydrated via an intermediate phase ($n = 0.9$, $P4/mmm$) to an anhydrous phase ($n = 0$, $I4/mmm$). Na^+ in these hydrated $NaLa_2Ti_2TaO_{10}$ phases occupies a face-shared octahedral site in the interlayer, surrounded by four water oxygens and two TaO_6 oxygens ($n = 2.0$) or by 2 water oxygens and four TaO_6 oxygens ($n = 1.0$). This is different from anhydrous $NaLa_2Ti_2TaO_{10}$, where Na^+ is located in the tetrahedral sites coordinated by four TaO_6 oxygens. It was pointed out that the formation of octahedral coordination around the Na^+ is a possible driving force for the smooth hydration. Judging from the structural similarity to the present $LiCa_2Ta_3O_{10}$ system, the displacement is possibly required to form the octahedral Li^+ coordination using a small number ($n < 1$) of water molecules in the interlayer.

Figure 5 shows SEM photographs of $LiCa_2Ta_3O_{10}$ before and after hydrothermal treatment at 180 °C. The prepared sample was composed of submicron crystallites with planar morphology, which is typical for layered structures. From TEM observation, it was confirmed that the basal plane of each crystallite was perpendicular to the (00*l*) planes. The morphology and crystal size were not changed after hydrothermal treatment. This is consistent with the measurement of BET surface area ($\leq 5\ m^2\ g^{-1}$).

Photocatalytic Activity of Hydrothermally Treated Li Phases. Photocatalytic water splitting was undertaken to study the effect of hydrothermal treatment. When anhydrous $LiCa_2Ta_3O_{10}$ alone dispersed in water was irradiated with UV light, the rates of gas evolved was low but enough to support stoichiometric water splitting (36 μmol-H_2 h^{-1} and 19 μmol-O_2 h^{-1}). The hydrothermal treatment at 160–180 °C decreased the activity; the rate of H_2 evolution was only $\leq 10\ \mu mol\ h^{-1}$. The effect of interlayer hydration is therefore negative for the Li phase alone. It is well-known that the photocatalytic water splitting is significantly enhanced by loading NiO_x as a co-catalyst,[1–3] which is impregnated onto photocatalysts using $Ni(NO_3)_2$ and subsequently heated in H_2 and then in O_2 to oxidize the surface of the Ni particles. The treatment yields core–shell-type NiO/Ni particles (NiO_x), which play the role of active site for H_2 evolution from water. However, this method cannot be applied to the present system, because a hydrated Li phase should loose water from the interlayer even at ≤ 200 °C (Fig. 2). To avoid this problem, the hydrothermal treatment was applied to the 0.5 wt % Ni-loaded $LiCa_2Ta_3O_{10}$, which was reduced in a flow of H_2 at 500 °C.

Figure 6 exhibits the photocatalytic gas evolution of 0.5 wt % Ni-loaded Li phase (a) as reduced by H_2 at 500 °C and (b) after subsequent hydrothermal treatment (160 °C, 12 h). For reduced sample (a), the stoichiometric evolution of H_2 and O_2 increased monotonically with the irradiation time, giving rise to the rates, 286 and 112 μmol h^{-1}, respectively. These values are lower than those for partially oxidized sample (356 μmol-H_2 h^{-1} and 194 μmol-O_2 h^{-1}) appearing in Table 1, evidencing the higher activity of NiO_x co-catalyst. More interestingly, the hydrothermal treatment increased the rates significantly to 708 μmol-H_2 h^{-1} and 333 μmol-O_2 h^{-1} (b), which are more than doubled for the partially reoxidized sample.

Table 2 summarizes the hydration number (*n*), interlayer distance (*d*), and photocatalytic activity of 0.5 wt % Ni/$LiCa_2Ta_3O_{10}$ after hydrothermal treatment under various conditions. The value of *n* was in the range 0.09–0.64, depending on temperature (160–180 °C) and time (2–18 h) for the hydrothermal treatment consistent with the values of interlayer distance, *d*. At 160 °C, activity increased with an increase of time for hydrothermal treatment in accordance with *n* and the highest activity of 2.5 times as large as that of untreated sample was obtained for 12 h. However, the activity decreased with further treatment. The tendency became more evident for treatment at higher temperatures; at 180 °C, the activity began to decrease even after 2 h. Thus, the hydrothermal treatment not only activates but also deactivates the Ni-loaded $LiCa_2Ta_3O_{10}$

Table 2. Effect of Hydrothermal Treatment on Photocatalytic Activity of 0.5 wt % Ni-Loaded $LiCa_2Ta_3O_{10}\cdot nH_2O$

Entry	Temp[a]/°C	Time[a]/h	n[b]/mol mol^{-1}	d[c]/nm	H_2[d]/μmol h^{-1}	O_2[d]/μmol h^{-1}
a	as prepared		0	1.41	286	112
b	160	2	0.09	1.42	578	274
c	160	6	0.26	1.45	638	279
d	160	12	0.44	1.48	708	333
e	160	18	0.45	1.51	494	266
f	170	2	0.16	1.44	531	243
g	170	6	0.37	1.47	632	303
h	170	12	0.55	1.49	424	188
i	170	18	0.62	1.50	507	225
j	180	2	0.27	1.45	666	328
k	180	6	0.43	1.49	509	232
l	180	12	0.64	1.52	287	124

a) Hydrothermal conditions. b) Hydration number. c) Interlayer spacing. d) Rates of photocatalytic gas evolution, photocatalyst 0.20 g, pure water 200 mL, inner-irradiation quartz vessel, 400-W high pressure Hg lamp. Ni-loaded photocatalysts were reduced in H_2 at 500 °C before hydrothermal treatment.

photocatalyst. Such a complicated effect can be explained considering the following two structural factors. First, increased photocatalytic activity is possibly associated with the hydration of interlayer space. As was pointed out for several ion-exchangeable layered oxide photocatalysts,[4,7,8,17] hydrated interlayer leads to more efficient water splitting. We also have to consider another factor concerning the chemical state of a Ni co-catalyst. Judging from the color of the photocatalyst that changed from gray to pale gray without loosing Ni loading, hydrothermal treatment seems to cause oxidation of Ni. This should be favorable to photocatalytic water splitting, when hydrothermal treatment may give rise to a partially oxidized surface layer (NiO_x) on the metal Ni particles, which is the most active co-catalyst. However, the activity will be destroyed when the loaded Ni is fully oxidized by hydrothermal treatment at higher temperature or over a long-term.

To determine which factors contribute to improved photocatalytic activity, the Na phase was next used as a reference in place of the Li phase. 0.5 wt % Ni-loaded Na phase ($NaCa_2Ta_3O_{10}$) after reduction in H_2 was hydrothermally treated under the optimized conditions, at 160 °C for 12 h. Unlike the Li phase, however, the rate of H_2 evolution decreased to 177 μmol h^{-1}, compared to 293 μmol h^{-1} achieved for Ni-loaded Na phase after reoxidation in O_2. Because the hydration of the Na phase was already completed by the smooth absorption of atmospheric moisture even before hydrothermal treatment, the decreased activity must result from excess oxidation of Ni co-catalyst. Taking these results into consideration, enhanced activity after hydrothermal treatment at 160 °C for 12 h is caused by the interlayer hydration of the Li phase. As we have pointed out in the hydrated $NaCa_2Ta_3O_{10}$ system, part of the interlayer water molecules would possibly be consumed by the photocatalytic reactions,[17] but its quantitative contribution to the overall reaction is not known in the present system. We need more evidence for the stoichiometric water splitting in the interlayer space to demonstrate the role of the interlayer as active site.

The photocatalytic activity after hydrothermal treatment was stable; the rates of gas evolution were constant without deactivation when the reaction was repeated. The stoichiometry of gas evolved, H_2/O_2, for the photocatalysts listed in Table 2 were in the range of 1.8–2.5. The largest deviation (2.5) from the theoretical value (2.0) was observed for Entry a, the sample of which was as reduced by H_2. This may be explained by the fact that part of evolved O_2 may be consumed to oxidize metallic Ni co-catalyst.

To summarize these results of the present study, hydrothermal treatment can yield $LiCa_2Ta_3O_{10}$ having a hydrated interlayer space, which is most active for photocatalytic water splitting in the presence of NiO_x co-catalyst. Our concept on activation by hydrating the interlayer achieved in the present study may have broad significance for various layered metal oxide photocatalyst systems having an anhydrous interlayer.

This work was financially supported by Core Research for Evolutional Science and Technology (CREST).

Supporting Information

Figure S1 is FT-IR spectra of $LiCa_2Ta_3O_{10}$. This material is available free of charge on the web at http://www.csj.jp/journals/bcsj/.

References

1 K. Domen, S. Naito, M. Soma, T. Ohnishi, K. Tamaru, *J. Chem. Soc., Chem. Commun.* **1980**, 543.

2 K. Domen, S. Naito, T. Onishi, K. Tamaru, *Chem. Phys. Lett.* **1982**, *92*, 433.

3 K. Domen, A. Kudo, T. Onishi, *J. Catal.* **1986**, *102*, 92.

4 A. Kudo, A. Tanaka, K. Domen, K. Maruya, K. Aika, T. Onishi, *J. Catal.* **1988**, *111*, 67.

5 Y. Inoue, T. Kubokawa, K. Sato, *J. Chem. Soc., Chem. Commun.* **1990**, 1298.

6 Y. Inoue, T. Niiyama, Y. Asai, K. Sato, *Chem. Commun.* **1992**, 579.

7 T. Takata, K. Shinohara, A. Tanaka, M. Hara, J. N. Kondo, K. Domen, *J. Photochem. Photobiol.* **1997**, *106*, 45.

8 T. Takata, Y. Furumi, K. Shinohara, A. Tanaka, M. Hara, J. N. Kondo, K. Domen, *Chem. Mater.* **1997**, *9*, 1063.

9 A. Kudo, H. Kato, *Chem. Lett.* **1997**, 867.
10 K. Sayama, K. Yasea, H. Arakawaa, K. Asakura, A. Tanaka, K. Domen, T. Onishi, *J. Photochem. Photobiol., A* **1998**, *114*, 125.
11 T. Ishihara, H. Nishiguchi, K. Fukamachi, T. Takita, *J. Phys. Chem. B* **1999**, *103*, 1.
12 M. Machida, J. Yabunaka, T. Kijima, *Chem. Commum.* **1999**, 1939.
13 A. Kudo, H. Kato, S. Nakagawa, *J. Phys. Chem. B* **2000**, *104*, 571.
14 M. Machida, J. Yabunaka, T. Kijima, *Mater. Chem.* **2000**, *12*, 812.
15 H. Kato, A. Kudo, *J. Phys. Chem. B* **2001**, *105*, 4285.
16 C. T. K. Thaminimulla, T. Takata, M. Hara, J. N. Kondo, K. Domen, *J. Catal.* **2001**, *196*, 362.
17 M. Machida, T. Mitsuyama, K. Ikeue, S. Matsushima, M. Arai, *J. Phys. Chem. B* **2005**, *109*, 7801.
18 K. Toda, T. Teranishi, Z. G. Ye, M. Sato, Y. Hinatsu, *Mater. Res. Bull.* **1999**, *34*, 971.
19 K. Toda, M. Sato, *J. Mater. Chem.* **1996**, *6*, 1067.
20 C. F. Bell, K. A. K. Lott, *Modern Approach to Inorganic Chemistry*, Butterworth Co., Ltd, London, **1991**.
21 K. Toda, K. Uematsu, M. Sato, *J. Ceram. Soc. Jpn.* **1997**, *105*, 482.
22 Y. S. Hong, C. H. Han, K. Kim, *J. Solid State Chem.* **2001**, *158*, 290.